Spin dephasing in a magnetic dipole field

C. H. Ziener,[1] T. Kampf,[2] G. Reents,[3] H.-P. Schlemmer,[1] and W. R. Bauer[4]
[1]*German Cancer Research Center (DKFZ), Im Neuenheimer Feld 280, 69120 Heidelberg, Germany*
[2]*University of Würzburg, Department of Experimental Physics 5, Am Hubland, 97074 Würzburg, Germany*
[3]*University of Würzburg, Department of Theoretical Physics 3, Am Hubland, 97074 Würzburg, Germany*
[4]*University of Würzburg, Department of Internal Medicine 1, Oberdürrbacher Straße 6, 97080 Würzburg, Germany*
(Received 14 June 2011; revised manuscript received 12 March 2012; published 16 May 2012)

Transverse relaxation by dephasing in an inhomogeneous field is a general mechanism in physics, for example, in semiconductor physics, muon spectroscopy, or nuclear magnetic resonance. In magnetic resonance imaging the transverse relaxation provides information on the properties of several biological tissues. Since the dipole field is the most important part of the multipole expansion of the local inhomogeneous field, dephasing in a dipole field is highly important in relaxation theory. However, there have been no analytical solutions which describe the dephasing in a magnetic dipole field. In this work we give a complete analytical solution for the dephasing in a magnetic dipole field which is valid over the whole dynamic range.

DOI: 10.1103/PhysRevE.85.051908 PACS number(s): 87.10.Ed, 87.64.kj, 87.61.Bj

I. INTRODUCTION

The effects of diffusion on free induction decay were first studied by Carr and Purcell by applying a linear gradient G additionally to the external magnetic field [1]. Thus, the local Larmor frequency is depending on the position in the form $\omega(x) = Gx$. The generalization to arbitrary inhomogeneous local magnetic fields was given by Torrey [2]. Formally, the Bloch-Torrey equation is equivalent to the Schrödinger equation in quantum mechanics, which has been analyzed for various kinds of potentials.

In the theory of spin dephasing, one-dimensional local magnetic fields are widely analyzed. However, only the one-dimensional linear gradient has been completely understood [3], while the analysis of dephasing in two-dimensional fields has been restricted to numerical solutions or approximations [4,5].

The field perturbation caused by magnetized objects can be expressed as a multipole expansion. In these expansions the lowest order is of main interest. For magnetic fields this is the dipole field. Often the magnetic field inhomogeneity varies the local field only in two directions, rendering the problem essentially two dimensional. Therefore, the lowest order multipole expansion is given by the two-dimensional dipole field. Thus, finding an analytical solution for the dephasing in this local field inhomogeneity is important as it serves as a generic model for understanding the basic physics of spin dephasing in two dimensions.

There are many situations where a two-dimensional dipole field provides a first-order model for the magnetic field inhomogeneity which, together with diffusion, governs the signal evolution, for example, in functional magnetic resonance [6,7]. In this case the blood-filled capillary has a different magnetic susceptibility than the surrounding tissue, leading to an inhomogeneous magnetic field around the capillary. Each capillary can be modeled by a cylinder and the local inhomogeneous magnetic field is a dipole field. Alterations of the measured signal can be used to monitor and quantify different parameters as blood oxygenation or blood supply of tissue. Furthermore, for susceptibility weighted imaging [8] the magnitude as well as the phase of the signal has to be known to analyze the images in terms of phase masks [9]. Thus, a profound knowledge of the signal evolution is mandatory.

In the following analysis we present an analytical solution of the Bloch-Torrey equation for dephasing in a two-dimensional magnetic dipole field in terms of an eigenfunction expansion. This solution is valid over the whole dynamic range and can be used to study and predict the time evolution of the transverse magnetization in experiments.

II. DIPOLE FIELD AND THE TIME EVOLUTION OF THE MAGNETIZATION

We consider a single cylindrical object with the radius R_{C} which has a tilt angle θ to the external magnetic field B_0 (see the left-hand side of Fig. 1). Due to the difference of the magnetic susceptibilities between the inside of the cylinder χ_i and the surrounding medium χ_e, the cylindrical object generates the local Larmor frequency which has the form of a two-dimensional dipole field [9]:

$$\omega(r,\phi) = \delta\omega R_{\mathrm{C}}^2 \frac{\cos(2\phi)}{r^2}, \qquad (1)$$

where r and ϕ are polar coordinates in a plane perpendicular to the axis of the cylinder (see the middle of Fig. 1). The shape of the dipole field is depicted in the right-hand side of Fig. 1. The characteristic frequency shift on the surface of the cylinder is given by $\delta\omega = \omega(r = R_{\mathrm{C}}, \phi = 0) = 2\pi\gamma|\chi_e - \chi_i|B_0 \sin^2(\theta)$, where γ is the gyromagnetic ratio of the proton [10]. The frequency shift $\delta\omega$ characterizes the strength of the susceptibility effects, while the diffusion of the spins around the cylinder is characterized by the diffusion coefficient D of the surrounding medium.

The transverse components $m_x(r,\phi,t)$ and $m_y(r,\phi,t)$ of the magnetization in the rotating frame can be combined to the complex magnetization $m(r,\phi,t) = m_x(r,\phi,t) + \mathrm{i}\, m_y(r,\phi,t)$. The time evolution of this complex magnetization is described by the Bloch-Torrey equation [2]

$$\partial_t m(r,\phi,t) = [D\Delta - i\omega(r,\phi) - 1/T_2]m(r,\phi,t)\,, \qquad (2)$$

where T_2 is the intrinsic spin-spin-relaxation time of the surrounding medium and Δ is the Laplace operator, which

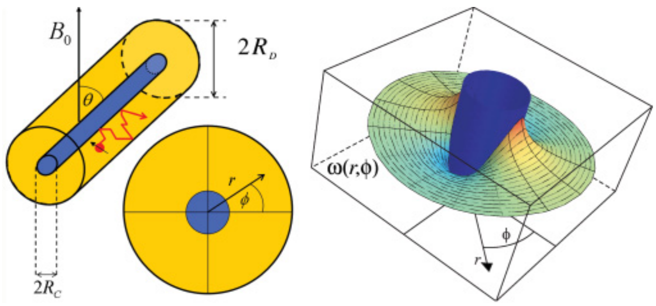

FIG. 1. (Color online) Cylindrical object and the surrounding dephasing cylinder in which the diffusion of the spin occurs (left). Cross section of the coaxial cylinders and coordinate system (middle). Two-dimensional dipole field around the cylinder (right) according to Eq. (1).

reads in two-dimensional polar coordinates $\Delta = r^{-1}\partial_r(r\partial_r) + r^{-2}\partial_{\phi\phi}$.

Initially the total magnetization is orientated in parallel to the external field in the z direction; that is, the transverse magnetization $m(r,\phi,t)$ vanishes. At the time $t = 0$, the application of a high-frequency pulse generates the transverse components $m_x(r,\phi,0)$ and $m_y(r,\phi,0)$, which can be combined to

$$m(r,\phi,0) = m_x(r,\phi,0) + i\, m_y(r,\phi,0) = m_0 = \text{const.} \quad (3)$$

At this time the transverse magnetization $m(r,\phi,t)$ takes its maximal value and decreases in the course of time due to the spin dephasing.

To determine the boundary conditions we consider a cylindrical dephasing volume with radius R_D coaxial to the cylindrical object; that is, the spins can diffuse in the interval $R_C \leqslant r \leqslant R_D$. At the surface of the cylindrical object as well as on the surface of the dephasing cylinder, we assume reflecting boundary conditions:

$$\partial_r m(r,\phi,t)|_{r=R_C} = 0 = \partial_r m(r,\phi,t)|_{r=R_D}, \quad (4)$$

which is explained in detail in [11,12]. The considered geometry as well as a scheme of the local magnetic dipole field is depicted in Fig. 1. While for impermeable objects the boundary condition at $r = R_C$ is strictly fulfilled, it also provides a good approximation if the water exchange between the magnetization of the inner cylinder and the dephasing volume is slow compared to the dephasing of the magnetization in the dephasing volume [13]. Furthermore the volume fraction of the inner cylinder should be small. The last condition ensures that the dominating part of the signal comes from the dephasing volume. Examples are blood-filled capillaries in the myocardium [11,14]. The reflecting boundary condition at the outer surface of the dephasing volume at $r = R_D$ is based on the model of Krogh [15]. Here the complete tissue is divided into similar cylindrical subvolumes that contain only one concentric inner capillary. These subvolumes are called supply volumes. When a diffusing spin leaves one of the subvolumes, it enters a neighboring one. This process can be replaced by reflecting the spin on the outer surface.

Furthermore, it is useful to introduce for abbreviation the characteristic time τ and the volume fraction η:

$$\tau = \frac{R_C^2}{D} \quad \text{and} \quad \eta = \frac{R_C^2}{R_D^2}. \quad (5)$$

Many approximative solutions are based on considering the limiting cases $\tau\delta\omega \ll 1$ (motional-narrowing regime) or $\tau\delta\omega \gg 1$ (slow-diffusion regime) [16]. In the myocardium the typical capillary radius is $R_C = 2.75\,\mu$m and the radius of the concentric supply cylinder is $R_D = 9.5\,\mu$m. In the supply cylinder the diffusion coefficient is $D = 1\,\mu\text{m}^2/\text{ms}$ and the intrinsic spin-spin-relaxation time is $T_2 = 57$ ms. At an external magnetic field strength of $B_0 = 1.5$ T, the characteristic frequency is $\delta\omega = 151\,\text{s}^{-1}$ and the parameter $\tau\delta\omega$ takes the value $\tau\delta\omega = 1.14$. Thus, neither the motional-narrowing nor the slow-diffusion regime is the underlaying dephasing regime. In the following analysis no approximations are necessary, and the result is valid over the whole dynamic range for all values of the ranging parameter $\tau\delta\omega$.

III. SOLUTION OF THE BLOCH-TORREY EQUATION

To find a solution of the Bloch-Torrey equation (2) for the local Larmor frequency (1) we use the ansatz

$$m(r,\phi,t) = T(t)R(r)\Phi(\phi), \quad (6)$$

which is justified by the linearity of Eq. (2). Separation of the angle-dependent part leads to the Mathieu differential equation [17]

$$\partial_{\phi\phi}\Phi_m(\phi) + \left[k_m^2 - i\,\tau\delta\omega\cos(2\phi)\right]\Phi_m(\phi) = 0 \quad (7)$$

with the angular eigenvalues k_m. Due to the symmetry of the two-dimensional dipole field the appropriate eigenfunctions are the π periodic, even Mathieu functions ce_{2m} [18]:

$$\Phi_m(\phi) = \text{ce}_{2m}(\phi, i\,\tau\delta\omega/2), \quad (8)$$

which obey the orthogonality relation

$$\int_0^{2\pi} d\phi\, \text{ce}_{2m}(\phi, i\,\tau\delta\omega/2)\text{ce}_{2m'}(\phi, i\,\tau\delta\omega/2) = \pi\delta_{mm'}. \quad (9)$$

The square of the angular eigenvalue k_m^2 is given by the characteristic value a_{2m} of the corresponding Mathieu function ce_{2m} with the required periodic behavior [17]:

$$k_m^2 = a_{2m}(i\,\tau\delta\omega/2). \quad (10)$$

In Appendix A we give a detailed description of the Mathieu functions and corresponding angular eigenvalues. In Fig. 2 the real and imaginary parts of k_m are visualized in dependence on the parameter $\tau\delta\omega$. Further properties and relations concerning the angular eigenvalues and angular eigenfunctions as well as details on their computation can be found in Appendix A.

For the radial function we obtain from the separation ansatz (6) the Bessel differential equation

$$\frac{\partial^2}{\partial r^2}R_{nm}(r) + \frac{1}{r}\frac{\partial}{\partial r}R_{nm}(r) + \left[\frac{\lambda_{nm}^2}{R_C^2} - \frac{k_m^2}{r^2}\right]R_{nm}(r) = 0$$

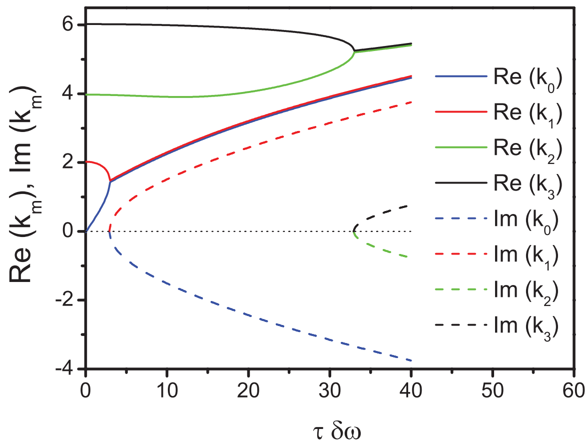

FIG. 2. (Color) Real part (solid lines) and imaginary part (dashed lines) of k_m obtained from Eq. (10). Beyond a branching point the corresponding two adjacent angular eigenvalues form complex conjugated pairs, e.g., $k_1 = k_0^*$ for $\tau\delta\omega \geqslant 2.94$. The first branching point is denoted as $p_0 \approx 2.94$. The positions of the first few branching points are given in Table I.

with the radial eigenvalues λ_{nm}^2. Regarding the reflecting boundary condition $\partial_r R_{nm}(r)|_{r=R_\mathrm{C}} = 0$ on the surface of the cylinder [see the left-hand side of Eq. (4)] the solution is a linear combination of the Bessel function and the Neumann function:

$$R_{nm}(r) = Y'_{k_m}(\lambda_{nm}) J_{k_m}\left(\frac{\lambda_{nm}}{R_\mathrm{C}} r\right) - J'_{k_m}(\lambda_{nm}) Y_{k_m}\left(\frac{\lambda_{nm}}{R_\mathrm{C}} r\right), \tag{11}$$

which obeys the orthogonality relation (see 11.4.2 in [19])

$$\frac{1}{R_\mathrm{C}^2}\int_{R_\mathrm{C}}^{R_\mathrm{D}} dr\, r R_{nm}(r) R_{n'm}(r) = N_{nm}\delta_{nn'} \quad \text{with} \tag{12}$$

$$N_{nm} = \frac{q_{nm}^2}{2}\left[\frac{1}{\eta} - \frac{k_m^2}{\lambda_{nm}^2}\right] - \frac{2}{\pi^2\lambda_{nm}^2}\left[1 - \frac{k_m^2}{\lambda_{nm}^2}\right] \quad \text{and} \tag{13}$$

$$q_{nm} = Y'_{k_m}(\lambda_{nm}) J_{k_m}\left(\frac{\lambda_{nm}}{\sqrt{\eta}}\right) - J'_{k_m}(\lambda_{nm}) Y_{k_m}\left(\frac{\lambda_{nm}}{\sqrt{\eta}}\right). \tag{14}$$

To obtain this result it is necessary to use Abel's identity for the Wronskian in the form

$$Y'_{k_m}(\lambda_{nm}) J_{k_m}(\lambda_{nm}) - J'_{k_m}(\lambda_{nm}) Y_{k_m}(\lambda_{nm}) = \frac{2}{\pi\lambda_{nm}} \tag{15}$$

(see 6.58 in [20]). With the help of this relation, from Eq. (11) it directly follows that $R_{nm}(R_\mathrm{C}) = 2/[\pi\lambda_{nm}]$. Furthermore, by comparison of Eqs. (11) and (14) one finds $R_{nm}(R_\mathrm{D}) = q_{nm}$. The normalization constants N_{nm} are dimensionless quantities and depend on the volume fraction η and the parameter $\tau\delta\omega$ only. A detailed analysis of the properties of the radial eigenfunctions is given in Appendix B.

The radial eigenvalues λ_{nm} are determined by the boundary condition $\partial_r R_{nm}(r)|_{r=R_\mathrm{D}} = 0$ at the surface of the concentric dephasing cylinder [see the right-hand side of Eq. (4)]:

$$0 = f_{k_m}(\lambda_{nm}) \quad \text{where} \tag{16}$$

$$f_{k_m}(\lambda) = Y'_{k_m}(\lambda) J'_{k_m}\left(\frac{\lambda}{\sqrt{\eta}}\right) - J'_{k_m}(\lambda) Y'_{k_m}\left(\frac{\lambda}{\sqrt{\eta}}\right). \tag{17}$$

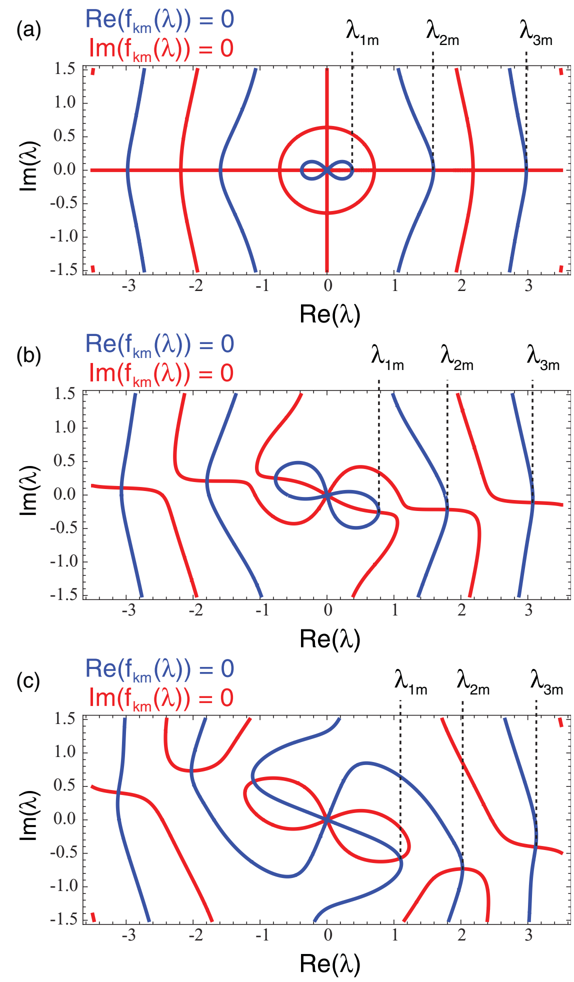

FIG. 3. (Color) Determination of the radial eigenvalues λ_{nm} as the crossing point of $\mathrm{Re}[f_{k_m}(\lambda)] = 0$ (blue line) and $\mathrm{Im}[f_{k_m}(\lambda)] = 0$ (red line) in the complex λ plane (exemplarily for $m = 0$ and $\eta = 0.1$). For $\tau\delta\omega = 2$ (a) the angular eigenvalue $k_m = 0.76$ is purely real and the crossing points lie on the real axis. For $\tau\delta\omega = 4$ (b) the angular eigenvalue $k_m = 1.58 - 0.59i$ is complex and therefore also the radial eigenvalues λ_{nm} are complex. For higher values of the parameter [i.e., $\tau\delta\omega = 10$ (c), $k_m = 2.27 - 1.51i$] the contour plots are more complicated.

To determine these radial eigenvalues, the contour plot of the implicit function $f_{k_m}(\lambda) = 0$ in the complex λ plane is considered (see Fig. 3). For $\tau\delta\omega \leqslant 2.94$ the angular eigenvalues k_m are purely real, and in Fig. 3(a) the real and imaginary parts of the function $f_{k_m}(\lambda) = 0$ are shown in the complex plane. In this case ($\tau\delta\omega \leqslant p_0 \approx 2.94$) also the radial eigenvalues λ_{nm} are purely real. The spectrum of the radial eigenvalues is visualized in Fig. 4. Further details concerning the calculation and properties of the radial eigenvalues and eigenfunctions are given in Appendix B.

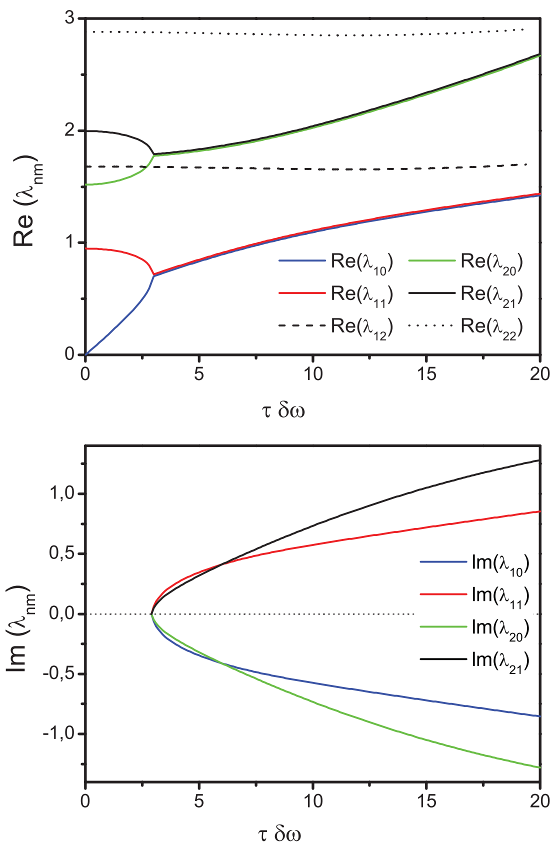

FIG. 4. (Color) Real part (top) and imaginary part (bottom) of the radial eigenvalues λ_{nm} as the solution of Eq. (16) for $\eta = 0.1$.

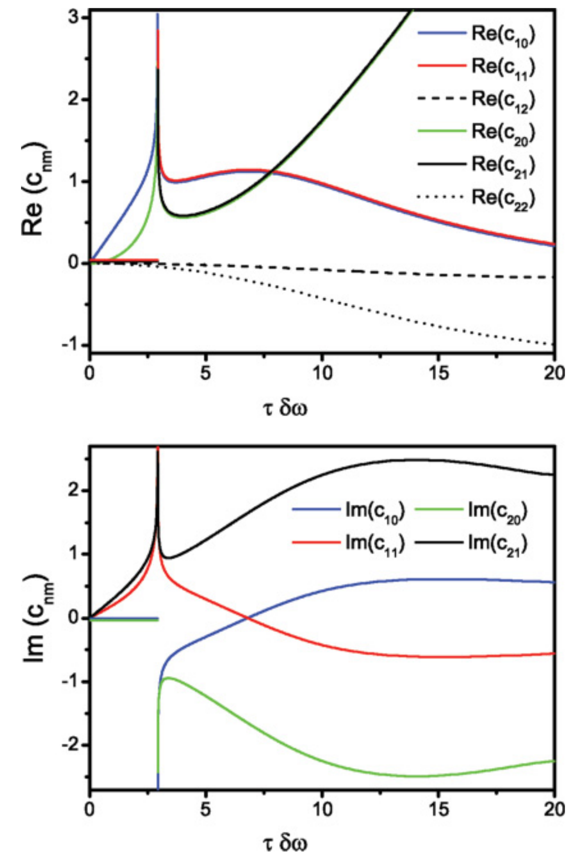

FIG. 5. (Color) Real part (top) and imaginary part (bottom) of the expansion coefficients c_{nm} obtained from Eq. (21) for $\eta = 0.1$.

The ansatz (6) finally leads to a differential equation for the time-dependent part:

$$\tau[\partial_t + 1/T_2]\, T_{nm}(t) = -\lambda_{nm}^2\, T_{nm}(t), \tag{18}$$

which has the solution

$$T_{nm}(t) = \mathrm{e}^{-t[\frac{\lambda_{nm}^2}{\tau} + \frac{1}{T_2}]}. \tag{19}$$

By introducing the three parts (8), (11), and (19) into the ansatz (6), the final solution of the Bloch-Torrey equation can be written as the sum over all eigenvalues in the form

$$\frac{m(\mathbf{r},t)}{m_0} = \mathrm{e}^{-\frac{t}{T_2}} \sum_{m=0}^{\infty}\sum_{n=1}^{\infty} c_{nm}\,\mathrm{ce}_{2m}(\phi, i\tau\delta\omega/2) R_{nm}(r)\mathrm{e}^{-\lambda_{nm}^2 \frac{t}{\tau}}, \tag{20}$$

where the function $R_{nm}(r)$ is given in Eq. (11). The coefficients c_{nm} can be determined using the initial value (3) and the orthogonality relations (9) and (12) (see Appendix C for a more detailed discussion):

$$c_{nm} = \pi A_0^{(2m)} \frac{2 s'_{1,k_m}(\lambda_{nm}) - \pi q_{nm} \frac{\lambda_{nm}}{\sqrt{\eta}} s'_{1,k_m}\left(\frac{\lambda_{nm}}{\sqrt{\eta}}\right)}{1 - k_m^2/\lambda_{nm}^2 - \pi^2 q_{nm}^2\left[\lambda_{nm}^2/\eta - k_m^2\right]/4} \tag{21}$$

with the Fourier coefficient

$$A_0^{(2m)} = \frac{1}{2\pi}\int_0^{2\pi} \mathrm{d}\phi\, \mathrm{ce}_{2m}(\phi, i\,\tau\delta\omega/2) \tag{22}$$

which can be obtained either by integration over the according Mathieu function [see Eq. (A7)] or by solving the matrix equation (A6), since $A_0^{(2m)}$ is proportional to the first element of the eigenvector corresponding to the angular eigenvalue k_m. The first derivative of the Lommel function [21] is

$$s'_{1,k_m}(x) = \frac{2x}{4 - k_m^2}\; {}_1F_2\left(2; 2 - \frac{k_m}{2}, 2 + \frac{k_m}{2}; -\frac{x^2}{4}\right),$$

where s'_{1,k_m} is given in terms of the generalized hypergeometric function. In Fig. 5 the expansion coefficients are visualized in dependence on the parameter $\tau\delta\omega$. A detailed derivation and discussion of the properties of the expansion coefficients c_{nm} is given in Appendix C. Interestingly, for $\tau\delta\omega \leqslant 2.94$ the radial eigenvalues λ_{nm} are purely real (see Fig. 4) and thus the magnetization decay is a linear combination of monoexponential decays without oscillations, since the temporal oscillating behavior is related to the imaginary part of the angular eigenvalues [see Eq. (19)]. For $\tau\delta\omega > 2.94$ the eigenvalues become complex and the imaginary part of the eigenvalues leads to an oscillating behavior of the magnetization. In Fig. 6 the transverse components $m_x(\mathbf{r},t) = \mathrm{Re}[m(\mathbf{r},t)]$ and $m_y(\mathbf{r},t) = \mathrm{Im}[m(\mathbf{r},t)]$ are shown for $t = 20$ ms after the excitation pulse.

IV. SUMMARY AND CONCLUSIONS

In summary, for spin dephasing in a two-dimensional magnetic dipole field the transverse components of the

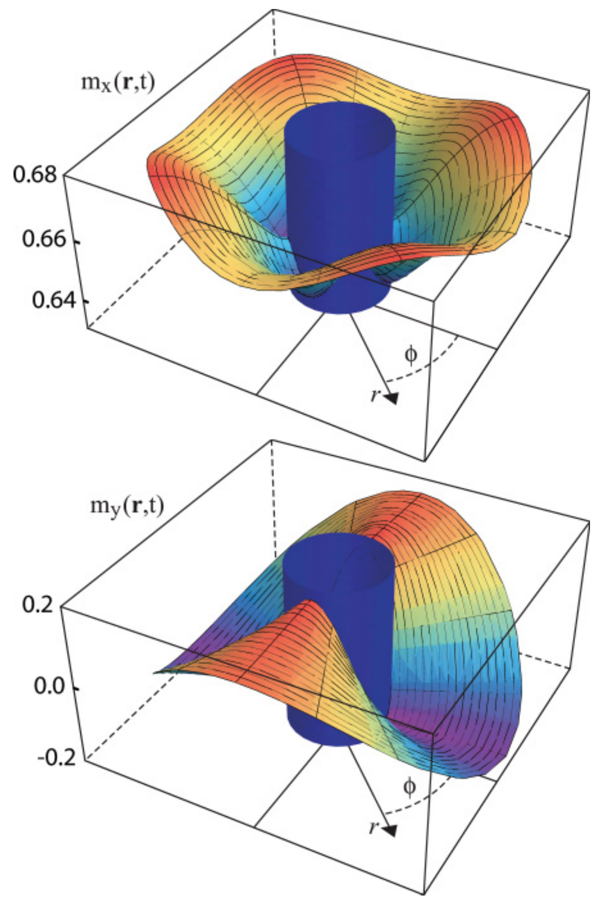

FIG. 6. (Color online) Transverse components of the magnetization around a capillary of the myocardium obtained from Eq. (20) using the parameters $R_{\rm C} = 2.75\,\mu$m, $R_{\rm D} = 9.5\,\mu$m, $D = 1\,\mu$m^2/ms, $T_2 = 57$ ms, $B_0 = 1.5$ T, and thus $\delta\omega = 151\,$s^{-1} with $\tau\delta\omega = 1.14$.

magnetization are analyzed. In analogy to the Schrödinger equation for a dipole potential, we give an analytical solution of the Bloch-Torrey equation in terms of an eigenfunction expansion. The analysis of the transverse magnetization is complicated by the fact that the inhomogeneity term is purely imaginary, in contradiction to quantum mechanics, where the potential is purely real. Thus, the eigenvalues are not purely real but complex. In the final solution the real part of the eigenvalues leads to exponential decay while the imaginary part causes an oscillatory behavior of the time evolution of the magnetization. The obtained result is highly relevant for spin dephasing in two-dimensional geometries, since the dipole component is the most important part of a multipole expansion of the inhomogeneous field. Furthermore, the validity of approximative solutions as well as random walk or Monte Carlo simulations can be tested by comparison with the analytical solution.

ACKNOWLEDGMENTS

This work was supported by grants from the Deutsche Forschungsgemeinschaft (SFB 688) and the Bundesministerium für Bildung und Forschung (BMBF01 EO1004).

APPENDIX A: PROPERTIES OF THE ANGULAR EIGENFUNCTIONS

Usually the Mathieu differential equation for the even π-periodic Mathieu functions is written in the form

$$\partial_{\phi\phi}\mathrm{ce}_{2m}(\phi,q) + [a_{2m} - 2q\cos(2\phi)]\mathrm{ce}_{2m}(\phi,q) = 0. \qquad \text{(A1)}$$

With $q = i\,\tau\delta\omega/2$ and $a_{2m} = k_m^2$ we obtain the differential equation

$$\partial_{\phi\phi}\mathrm{ce}_{2m}(\phi,i\,\tau\delta\omega/2) + \left[k_m^2 - i\,\tau\delta\omega\cos(2\phi)\right] \times \mathrm{ce}_{2m}(\phi,i\,\tau\delta\omega/2) = 0, \qquad \text{(A2)}$$

which coincides with the differential equation (7) obtained from the separation ansatz. The Mathieu functions can be written in a Fourier series,

$$\mathrm{ce}_{2m}(\phi,i\,\tau\delta\omega/2) = \sum_{u=0}^{\infty} A_{2u}^{(2m)}\cos(2u\phi), \qquad \text{(A3)}$$

which reflects the symmetry $\mathrm{ce}_{2m}(\phi,i\,\tau\delta\omega/2) = \mathrm{ce}_{2m}(-\phi,i\,\tau\delta\omega/2)$. Due to the orthogonality relation (9), the Fourier coefficients have to obey the normalization

$$2\left[A_0^{(2m)}\right]^2 + \sum_{u=1}^{\infty}\left[A_{2u}^{(2m)}\right]^2 = 1. \qquad \text{(A4)}$$

The eigenfunctions $\mathrm{ce}_{2m}(\phi,i\,\tau\delta\omega/2)$ exhibit only for certain angular eigenvalues k_m the required periodicity. For a given parameter $\tau\delta\omega$ the angular eigenvalues k_m and the Fourier coefficients $A_{2u}^{(2m)}$ of the Mathieu functions can be determined by solving the recurrence relation (see 20.2.5–20.2.7 in [19] with $q = i\tau\delta\omega/2$ and $k_m^2 = a_{2m}$):

$$\begin{aligned} 2k_m^2 A_0^{(2m)} &= i\tau\delta\omega A_2^{(2m)}, \\ 2\left[k_m^2 - 4\right]A_2^{(2m)} &= i\tau\delta\omega\left[2A_0^{(2m)} + A_4^{(2m)}\right], \qquad \text{(A5)} \\ 2\left[k_m^2 - 4u^2\right]A_{2u}^{(2m)} &= i\tau\delta\omega\left[A_{2u-2}^{(2m)} + A_{2u+2}^{(2m)}\right] \quad \text{for} \quad u \geqslant 2. \end{aligned}$$

For numerical evaluation it is convenient to write the recurrence relation in terms of a matrix equation:

$$\begin{pmatrix} 0 & \frac{i\tau\delta\omega}{\sqrt{2}} & & & & & \\ \frac{i\tau\delta\omega}{\sqrt{2}} & 4 & \frac{i\tau\delta\omega}{2} & & & & \\ & \frac{i\tau\delta\omega}{2} & 16 & \frac{i\tau\delta\omega}{2} & & & \\ & & \frac{i\tau\delta\omega}{2} & 36 & \frac{i\tau\delta\omega}{2} & & \\ & & & \ddots & \ddots & \ddots & \\ & & & & \frac{i\tau\delta\omega}{2} & 4u^2 & \frac{i\tau\delta\omega}{2} \\ & & & & & & \ddots \end{pmatrix} \begin{pmatrix} \sqrt{2}A_0^{(2m)} \\ A_2^{(2m)} \\ A_4^{(2m)} \\ A_6^{(2m)} \\ \vdots \\ A_{2u}^{(2m)} \\ \vdots \end{pmatrix} = k_m^2 \begin{pmatrix} \sqrt{2}A_0^{(2m)} \\ A_2^{(2m)} \\ A_4^{(2m)} \\ A_6^{(2m)} \\ \vdots \\ A_{2u}^{(2m)} \\ \vdots \end{pmatrix}. \qquad \text{(A6)}$$

TABLE I. Positions of the branching points.

l	0	1	2	3
p_l	2.94	32.94	95.62	190.96
$k_{2l} = k_{2l+1}$	1.45	5.23	8.98	12.73

Therefore, the determination of the angular eigenvalues translates in an eigenvalue problem of the resulting tridiagonal infinite matrix.

The Fourier coefficients of the Fourier series in Eq. (A3) are important in the following analysis (see (5.3.4) in [22]):

$$A_{2u}^{(2m)} = \frac{1}{\pi[1+\delta_{0u}]}\int_0^{2\pi} d\phi \cos(2u\phi)\mathrm{ce}_{2m}\left(\phi, i\frac{\tau\delta\omega}{2}\right). \tag{A7}$$

These first Fourier coefficients obey the Parseval relation

$$\sum_{m=0}^{\infty}\left[A_0^{(2m)}\right]^2 = \frac{1}{2} \tag{A8}$$

(see Eq. (20) in [18] and Eq. (18.4.1) in [22]). This relation can be used to estimate the number of coefficients necessary to obtain the required accuracy in numerical calculations.

The angular eigenvalues k_m are purely real until they reach their branching point. Behind the branching point two adjacent angular eigenvalues become complex conjugated. For example, the lowest angular eigenvalues k_0 and k_1 are purely real for $\tau\delta\omega < p_0$. At the branching point $\tau\delta\omega = p_0$ both these angular eigenvalues coincide ($k_0 = k_1 = 1.45$). Behind the branching point $\tau\delta\omega > p_0$ yields $k_0 = k_1^*$. This is visualized in Fig. 2, and the positions of the lowest branching points are given in Table I.

Approximately the branching points are located at the positions $p_l = 16.336l^2 + 13.64l + 2.94$. In general one finds for the complex conjugated pairs of the angular eigenvalues

$$k_{2l+1} = k_{2l}^* \quad \text{for} \quad \tau\delta\omega > p_l. \tag{A9}$$

Similar relations are valid for the Mathieu functions

$$\mathrm{ce}_{4l+2}(\phi, i\tau\delta\omega/2) = \mathrm{ce}_{4l}^*(\pi/2-\phi, i\tau\delta\omega/2) \quad \text{for} \quad \tau\delta\omega > p_l, \tag{A10}$$

and their Fourier coefficients

$$A_{2u}^{(4l+2)} = [-1]^u A_{2u}^{(4l)*} \quad \text{for} \quad \tau\delta\omega > p_l\,. \tag{A11}$$

Furthermore, the angular eigenvalues obey the relation

$$\sum_{m=0}^{\infty}\left[k_m^2 - 4m^2\right] = 0, \tag{A12}$$

which directly follows from Eq. 28.7.1 in [23].

APPENDIX B: PROPERTIES OF THE RADIAL EIGENFUNCTIONS

For calculation of the radial eigenvalues λ_{nm} as a solution of $f_{k_m}(\lambda_{nm}) = 0$ [see Eq. (16)] it is useful to know the properties of the function $f_{k_m}(\lambda)$ defined in Eq. (17):

$$f_{k_m}(\lambda) = f_{k_m}(-\lambda), \tag{B1}$$

$$f_{k_m}(\lambda) = f_{-k_m}(\lambda), \quad \text{and} \tag{B2}$$

$$f_{k_m^*}(\lambda) = f_{k_m}^*(\lambda^*). \tag{B3}$$

According to Eq. (A9) the angular eigenvalues are complex conjugated behind their branching point, for example, $k_1 = k_0^*$ for $\tau\delta\omega > p_0 \approx 2.94$ (see Fig. 2). From Eq. (B3) it follows that the eigenvalues of the radial eigenfunctions are also complex conjugated: $\lambda_{n1} = \lambda_{n0}^*$ for $\tau\delta\omega > p_0 \approx 2.94$. In general it follows from Eq. (A9) that the relation

$$\lambda_{n\,2l+1} = \lambda_{n\,2l}^* \quad \text{for} \quad \tau\delta\omega > p_l\,, \tag{B4}$$

which translates to the eigenfunctions

$$R_{n\,2l+1}(r) = R_{n\,2l}^*(r) \quad \text{for} \quad \tau\delta\omega > p_l\,. \tag{B5}$$

All angular eigenvalues k_m are purely real for $\tau\delta\omega \leqslant p_0$. In Fig. 3(a) the real and imaginary parts of the function $f_{k_m}(\lambda) = 0$ are shown. One can see that for $\tau\delta\omega \leqslant p_0$ the radial eigenvalues λ_{nm} are solely real too.

Behind the first branching point (i.e., for $\tau\delta\omega > p_0$) the angular eigenvalues k_m can become complex. In Figs. 3(b) and 3(c) the real and imaginary parts of the implicit function $f_{k_m}(\lambda) = 0$ for a complex angular eigenvalue k_m are shown. Obviously, the radial eigenvalues λ_{nm} are complex too.

The first radial eigenvalue which is determined by the eigenvalue equation (16) can be obtained by the Taylor expansion of the function $f_{k_m}(\lambda)$ for small arguments:

$$\lambda_{1m}^2 \approx \frac{4\eta k_m\left[1-k_m^2\right]\left[\eta^{k_m}-1\right]}{\left[k_m^2+k_m-2\right][1-\eta]\left[1+\eta^{k_m}\right] - 2k_m\left[\eta^{k_m}-\eta\right]}. \tag{B6}$$

For small values of the angular eigenvalue k_m this expression can be simplified further. Finally one obtains the approximations of the desired radial eigenvalues:

$$\lambda_{1m} \approx k_m \frac{\eta \ln(\eta)}{\eta - 1} \quad \text{for} \quad n = 1 \quad \text{and} \tag{B7}$$

$$\lambda_{nm} \approx \pi\sqrt{\eta}\frac{n-1}{1-\sqrt{\eta}} + \frac{1-\sqrt{\eta}}{n-1}\frac{4k_m^2+3}{8\pi} \quad \text{for} \quad n \geqslant 2, \tag{B8}$$

where (B7) is derived from the Taylor expansion (B6), while the relation (B8) is described in paragraph 10.21.49 of [23]. Approximations for the first and further radial eigenvalues in the case of large volume fractions are described in Eqs. (A.4) and (A.5) of [24]. In general the radial eigenvalues λ_{nm} can be determined numerically from Eq. (16). To improve the stability and convergence of the numerical root search, the approximations given in relations (B7) and (B8) can be used as initial values. The spectrum of the lowest radial eigenvalues is shown in Fig. 4.

APPENDIX C: PROPERTIES OF THE EXPANSION COEFFICIENTS

The expansion coefficients c_{nm} can be determined by exploiting the initial condition $m(r,\phi,t=0)=m_0$ and the orthogonality relations (9) and (12):

$$c_{nm} = \frac{2A_0^{(2m)}}{N_{nm}R_\mathrm{C}^2}\int_{R_\mathrm{C}}^{R_\mathrm{D}} dr\, r\, R_{nm}(r)\,, \tag{C1}$$

where the Fourier coefficient $A_0^{(2m)}$ can be obtained from matrix equation (A6) or from the integral given in Eq. (A7). The normalization factor N_{nm} is given in Eq. (13). To determine the expansion coefficients the integral in Eq. (C1) has to be solved. Using the volume fraction $\eta = R_\mathrm{C}^2/R_\mathrm{D}^2$ we obtain with the help of Eq. (5) in paragraph 10.74 in [21]

$$\begin{aligned} M_{nm} &= \frac{1}{R_\mathrm{C}^2}\int_{R_\mathrm{C}}^{R_\mathrm{D}} dr\, r\, R_{nm}(r) \\ &= \frac{q_{nm}}{\lambda_{nm}\sqrt{\eta}} s'_{1,k_m}\left(\frac{\lambda_{nm}}{\sqrt{\eta}}\right) - \frac{2}{\pi\lambda_{nm}^2}s'_{1,k_m}(\lambda_{nm}), \end{aligned} \tag{C2}$$

where q_{nm} is given in Eq. (14) and

$$\begin{aligned} s_{\mu,k_m}(x) &= \frac{x^{\mu+1}}{[\mu+1]^2-k_m^2} \\ &\quad\times {}_1F_2\left(1;\frac{\mu+3-k_m}{2},\frac{\mu+3+k_m}{2};-\frac{x^2}{4}\right) \end{aligned} \tag{C3}$$

is the Lommel function [25,26], with ${}_1F_2$ as the generalized hypergeometric function. An equivalent definition of the Lommel function can be found in 11.9.3 in [23]. Instead of the Lommel function s it is possible to use the second Lommel function S too (see 11.9.5 in [23]). With the help of relation $s_{1,k_m}(x) = 1 + k_m^2 s_{-1,k_m}(x)$ (see [26], p. 112) it follows that

$$s'_{1,k_m}(x) = \frac{2x}{4-k_m^2}\,{}_1F_2\left(2;2-\frac{k_m}{2},2+\frac{k_m}{2};-\frac{x^2}{4}\right). \tag{C4}$$

Finally one obtains for the expansion coefficients

$$\begin{aligned} c_{nm} &= 2A_0^{(2m)}\frac{M_{nm}}{N_{nm}} \\ &= 4\pi\eta A_0^{(2m)}\lambda_{nm}^2\frac{2s'_{1,k_m}(\lambda_{nm}) - \pi q_{nm}\frac{\lambda_{nm}}{\sqrt{\eta}}s'_{1,k_m}\left(\frac{\lambda_{nm}}{\sqrt{\eta}}\right)}{4\eta\left[\lambda_{nm}^2-k_m^2\right]-\pi^2\lambda_{nm}^2q_{nm}^2\left[\lambda_{nm}^2-\eta k_m^2\right]}. \end{aligned} \tag{C5}$$

The expansion coefficients c_{nm} depend on the volume fraction η and the parameter $\tau\delta\omega$ only. The properties of the radial eigenvalues in Eq. (B4) translate to the expansion coefficients

$$c_{n\,2l+1} = c_{n\,2l}^* \quad \text{for} \quad \tau\delta\omega > p_l\,. \tag{C6}$$

In Fig. 5 the expansion coefficients c_{nm} in dependence on the parameter $\tau\delta\omega$ are shown. Considering the magnetization on the surface of the capillary one finds by substituting Eq. (15) in Eq. (20)

$$m(r=R_C,\phi,t) = \frac{2m_0}{\pi}\sum_{m=0}^{\infty}\sum_{n=1}^{\infty}\frac{c_{nm}}{\lambda_{nm}}\mathrm{ce}_{2m}(\phi)\mathrm{e}^{-t\left[\frac{\lambda_{nm}^2}{\tau}+\frac{1}{T_2}\right]}. \tag{C7}$$

Since at $t=0$ the magnetization takes the constant initial value $m(r=R_\mathrm{C},\phi,t=0)=m_0$ the orthogonality relation (9) in combination with the first Fourier coefficients from Eq. (A7) yields the relation

$$\begin{aligned} &\sum_{n=1}^{\infty}\frac{M_{nm}}{\lambda_{nm}N_{nm}} = \frac{\pi}{2} \quad \text{or} \\ &\sum_{n=1}^{\infty}\frac{2s'_{1,k_m}(\lambda_{nm}) - \pi q_{nm}\frac{\lambda_{nm}}{\sqrt{\eta}}s'_{1,k_m}\left(\frac{\lambda_{nm}}{\sqrt{\eta}}\right)}{4\eta\left[\lambda_{nm}^2-k_m^2\right]-\pi^2\lambda_{nm}^2q_{nm}^2\left[\lambda_{nm}^2-\eta k_m^2\right]}\lambda_{nm} = \frac{1}{4\eta}. \end{aligned} \tag{C8}$$

This relation can be used to check if a sufficient number of coefficients is used in numerical calculations. An analogous treatment is possible if the magnetization on the surface of the dephasing cylinder at $r = R_\mathrm{D}$ is considered. Applying the definition (14) to Eq. (20) yields

$$m(r=R_\mathrm{D},\phi,t) = m_0\sum_{m=0}^{\infty}\sum_{n=1}^{\infty}c_{nm}q_{nm}\mathrm{ce}_{2m}(\phi)\mathrm{e}^{-t\left[\frac{\lambda_{nm}^2}{\tau}+\frac{1}{T_2}\right]}. \tag{C9}$$

As the magnetization at $t=0$ takes the value $m(r=R_\mathrm{D},\phi,t=0)=m_0$ too, one similarly obtains with the orthogonality relation (9) and the first Fourier coefficients (A7) the relation

$$\begin{aligned} &\sum_{n=1}^{\infty}\frac{q_{nm}M_{nm}}{N_{nm}} = 1 \quad \text{or} \\ &\sum_{n=1}^{\infty}\frac{2s'_{1,k_m}(\lambda_{nm}) - \pi q_{nm}\frac{\lambda_{nm}}{\sqrt{\eta}}s'_{1,k_m}\left(\frac{\lambda_{nm}}{\sqrt{\eta}}\right)}{4\eta[\lambda_{nm}^2-k_m^2]-\pi^2\lambda_{nm}^2q_{nm}^2[\lambda_{nm}^2-\eta k_m^2]}q_{nm}\lambda_{nm}^2 = \frac{1}{2\pi\eta}. \end{aligned} \tag{C10}$$

Integrating Eq. (20) at $t=0$ over the dephasing volume ($R_\mathrm{C}\leqslant r\leqslant R_\mathrm{D}$ and $0\leqslant\phi\leqslant 2\pi$) one finds with Eq. (A7) and Eq. (C1) the Parseval relation

$$\sum_{m=0}^{\infty}\sum_{n=1}^{\infty}c_{nm}^2N_{nm} = \frac{1}{\eta}-1\,. \tag{C11}$$

This relation can also be used to check if the summation over n covers a sufficient number of coefficients for a desired numerical accuracy. An analogous relation for the second summation index m can be found with the relation (A8).

The result for the magnetization $m(r,\phi,t)$ in Eq. (20) is valid for any value of the parameter $\tau\delta\omega$. However, the individual quantities in Eq. (20) exhibit specific symmetry relations for $\tau\delta\omega > p_0$. Using the symmetry properties of the Mathieu functions [see Eq. (A10)], the radial eigenvalues [see Eq. (B4)], the radial eigenfunctions [see Eq. (B5)], as well as the properties of the expansion coefficients [see Eq. (C6)], the final result for the magnetization given in Eq. (20) can be written in the form

$$\frac{m(r,\phi,t)}{m_0} = \sum_{m=0}^{l}\sum_{n=1}^{\infty}\left[c_{n\,2m}\mathrm{ce}_{4m}(\phi)R_{n\,2m}(r)\mathrm{e}^{-t[\frac{\lambda_{n\,2m}^2}{\tau}+\frac{1}{T_2}]} + c_{n\,2m}^{*}\mathrm{ce}_{4m}^{*}\left(\frac{\pi}{2}-\phi\right)R_{n\,2m}^{*}(r)\mathrm{e}^{-t[\frac{\lambda_{n\,2m}^{2*}}{\tau}+\frac{1}{T_2}]}\right] + \sum_{m=2l+2}^{\infty}\sum_{n=1}^{\infty}c_{nm}\mathrm{ce}_{2m}(\phi)R_{nm}(r)\mathrm{e}^{-t[\frac{\lambda_{nm}^2}{\tau}+\frac{1}{T_2}]} \quad \text{for} \quad p_l < \tau\delta\omega < p_{l+1}. \tag{C12}$$

Similarly to relation (C11) one finds by integrating $m(r,\phi,t)$ over the dephasing volume the relation

$$2\sum_{m=0}^{l}\sum_{n=1}^{\infty}\mathrm{Re}\left(c_{n\,2m}^2 N_{n\,2m}\right) + \sum_{m=2l+2}^{\infty}\sum_{n=1}^{\infty}c_{nm}^2 N_{nm} = \frac{1}{\eta} - 1 \quad \text{for} \quad p_l < \tau\delta\omega < p_{l+1}\,. \tag{C13}$$

[1] H. Y. Carr, and E. M. Purcell, Phys. Rev. **94**, 630 (1954).
[2] H. C. Torrey, Phys. Rev. **104**, 563 (1956).
[3] S. D. Stoller, W. Happer, and F. J. Dyson, Phys. Rev. A **44**, 7459 (1991).
[4] C. H. Ziener, T. Kampf, G. Melkus, V. Herold, T. Weber, G. Reents, P. M. Jakob, and W. R. Bauer, Phys. Rev. E **76**, 031915 (2007).
[5] C. H. Ziener, S. Glutsch, P. M. Jakob, and W. R. Bauer, Phys. Rev. E **80**, 046701 (2009).
[6] S. Ogawa, T. M. Lee, A. R. Kay, and D. W. Tank, Proc. Natl. Acad. Sci. USA **87**, 9868 (1990).
[7] D. G. Norris, NMR Biomed. **14**, 77 (2001).
[8] E. M. Haacke, Y. Xu, Y. C. Cheng, and J. R. Reichenbach, Magn. Reson. Med. **52**, 612 (2004).
[9] J. R. Reichenbach and E. M. Haacke, NMR Biomed. **14**, 453 (2001).
[10] W. R. Bauer, W. Nadler, M. Bock, L. R. Schad, C. Wacker, A. Hartlep, and G. Ertl, Magn. Reson. Med. **41**, 51 (1999).
[11] W. R. Bauer, W. Nadler, M. Bock, L. R. Schad, C. Wacker, A. Hartlep, and G. Ertl, Phys. Rev. Lett. **83**, 4215 (1999).
[12] C. H. Ziener, T. Kampf, V. Herold, P. M. Jakob, W. R. Bauer, and W. Nadler, J. Chem. Phys. **129**, 014507 (2008).
[13] C. H. Ziener, W. R. Bauer, G. Melkus, T. Weber, V. Herold, and P. M. Jakob, Magn. Reson. Imaging **24**, 1341 (2006).
[14] K. M. Donahue, D. Burstein, W. J. Manning, and M. L. Gray, Magn. Reson. Med. **32**, 66 (1994).
[15] A. Krogh, J. Physiol. **52**, 409 (1919).
[16] D. S. Grebenkov, Rev. Mod. Phys. **79**, 1077 (2007).
[17] N. W. McLachlan, *Theory and Application of Mathieu Functions* (Dover, New York, 1964).
[18] A. Seeger, Hyperfine Interact. **105**, 151 (1997).
[19] M. Abramowitz and I. A. Stegun, *Handbook of Mathematical Functions with Formulas, Graphs, and Mathematical Tables* (Dover, New York, 1972).
[20] M. R. Spiegel, *Fourier Analysis* (McGraw-Hill, London, 1976).
[21] G. N. Watson, *A Treatise on the Theory of Bessel Functions* (Cambridge University Press, Cambridge, 1995).
[22] F. P. Mechel, *Mathieu Functions* (S. Hirzel Verlag, Stuttgart, 1997).
[23] F. W. J. Olver, D. W. Lozier, R. F. Boisvert, and C. W. Clark. *NIST Handbook of Mathematical Functions* (Cambridge University Press, Cambridge, 2010).
[24] H. P. W. Gottlieb, J. Austral. Math. Soc. Ser. B **26**, 293 (1985).
[25] E. Lommel, Math. Ann. **9**, 425 (1875).
[26] W. Magnus, F. Oberhettinger, and R. P. Soni. *Formulas and Theorems for the Special Functions of Mathematical Physics* (Springer, Berlin, 1966).